

Multicomponent Polycoupling of Internal Diynes, Aryl Diiodides, and Boronic Acids to Functional Poly(tetraarylethene)s

Yajing Liu,^{†,‡} Jesse Roose,[‡] Jacky W. Y. Lam,^{†,‡} and Ben Zhong Tang^{*,†,‡,§}

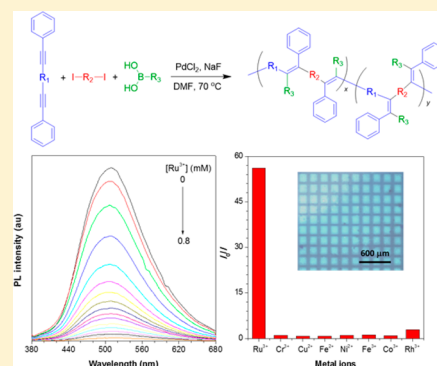
[†]HKUST-Shenzhen Research Institute, No. 9 Yuexing first RD, South Area, Hi-tech Park, Nanshan, Shenzhen 518057, China

[‡]Department of Chemistry, Hong Kong Branch of National Engineering Research Center for Tissue Restoration Reconstruction, Division of Life Science, State Key Laboratory of Molecular Neuroscience, Institute for Advanced Study, Institute of Molecular Functional Materials, and Division of Biomedical Engineering, The Hong Kong University of Science and Technology, Clear Water Bay, Kowloon, Hong Kong, China

[§]Guangdong Innovative Research Team, SCUT-HKUST Joint Research Laboratory, State Key Laboratory of Luminescent Materials and Devices, South China University of Technology, Guangzhou 510640, China

Supporting Information

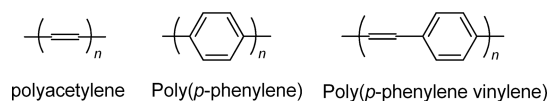
ABSTRACT: This paper describes the development of a new three-component polymerization route to functional poly(tetraarylethene)s (PTAEs). The polycoupling reactions of internal diynes, aryl diiodides, and arylboronic acids proceed smoothly in the presence of PdCl₂ and NaF at 70 °C in dimethylformamide, generating PTAEs with promising molecular weights in high yields from different monomers. Most of the PTAEs are soluble in common organic solvents and are thermally stable. Some of the PTAEs exhibit the phenomenon of aggregation-induced emission: their light emission in solution is enhanced by aggregate formation. The tetraphenylethene-containing PTAE can function as a fluorescent chemosensor for detecting Ru³⁺ ions with high sensitivity and specificity. It is also a promising material for the fabrication of fluorescent pattern by photolithography process. All the PTAEs possess good film-forming ability and their thin films exhibit high refractive index (RI = 1.7751–1.6382) at 632.8 nm, whose values are higher than those of commercial polymers such as polycarbonate and polystyrene.



INTRODUCTION

Research on conjugated polymers has been a classic topic for many decades because of their distinct properties and promising applications.¹ Among them, polyacetylene, poly(*p*-phenylene), and poly(*p*-phenylenevinylene) (PPV) are the most classical ones (Scheme 1). Despite their outstanding

Scheme 1. Structures of Polyacetylene, Poly(*p*-phenylene), and PPV



features like electrical conductivity, these rigid rod-like polymers are not suitable for most real-world applications because they all suffer from infusibility and hence low processability. Taking PPV as an example, many approaches have been developed to improve its tractability and solubility through, for example, the precursor routes,² postpolymerization modification,³ and attachment of pendant groups to its backbone.⁴ However, both pre- and postmodification methods make the preparation process complicated and may lead to defects in the polymer structure. Functional pendants, on the contrary, can not only improve the processability of PPV but

also equip the polymer with multiple functions. Thus, it is widely utilized in PPV modification.

Various reactions have been developed to synthesize substituted PPVs with alkyl, alkoxy, or phenyl side chains, such as Wittig coupling,⁵ Knoevenagel condensation⁶ and Heck coupling⁷ reactions. Polymers generated from Wittig-type polycoupling of an aryl dialdehyde and a diylide usually suffer from low molecular weights, broad polydispersity, and poor control of diastereoselectivity. Although Knoevenagel polycondensation of phenylenediacetonitrile with an aryl dialdehyde can yield polymers with high molecular weights, side reactions such as hydrolysis of nitrile groups are a common problem. Because of its high efficiency, Heck polycoupling of aromatic dihalides with dialkenes or ethenes appears to be the method of choice to furnish a myriad of different PPVs. Since alkenes with substituents are limited, the pendants of the corresponding polymers are thus generally attached on the phenyl rings.

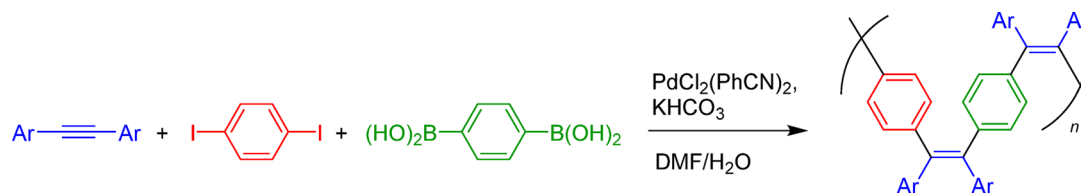
In 2003, Larock and co-workers reported a palladium-catalyzed one-step, one-pot three-component coupling reaction of aryl iodide, internal alkyne and aryl diboronic acid, giving tetrasubstituted olefins in excellent yields under mild conditions

Received: September 5, 2015

Revised: October 31, 2015

Published: November 9, 2015

Scheme 2. Polycoupling of Diarylacetylene, Diiodobenzene, and Benzene-1,4-Diboronic Acid



with high regio- and stereoselectivity.⁸ Based on Larock's work, Tomita⁹ developed the corresponding three-component polymerization of aryl dihalide, aryl diboronic acid and diarylacetylene catalyzed by $\text{PdCl}_2(\text{PhCN})_2$ and KHCO_3 in 2007 (Scheme 2). Poly(tetraarylethene) (PTAE) with good solubility in common organic solvents was successfully obtained, but its molecular weight was rather low ($M_n = 2600$). The polymerization was carried out at $100\text{ }^\circ\text{C}$ for 24 h, which may set a limit on the monomer scope. Therefore, in this paper, we aim to modify this polymerization and develop it into a versatile strategy to synthesize soluble PTAEs with higher molecular weights and variable structures under mild conditions.

On the basis of our experience in developing novel synthetic routes to functional polymers,¹⁰ we finally found better conditions for synthesizing such polymers. PTAEs with fully or partially conjugated structures and high molecular weights of up to 18000 can be readily synthesized from readily available internal diynes and other commercially available monomers in the presence of PdCl_2 and NaF in dimethylformamide (DMF) at $70\text{ }^\circ\text{C}$ within 18 h. Since the tetraarylethene moieties generated *in situ* are typical chromophores with aggregation-induced emission (AIE) features,¹¹ the obtained PTAEs may be AIE-active as well. Indeed, some of the PTAEs exhibit more intense fluorescence in the aggregated state than their solutions. Thus, they are promising as solid-state emission materials and may find applications as imaging agents or fluorescent sensors.

EXPERIMENTAL SECTION

Materials and Instruments. Aryl diiodides, arylboronic acids, and other reagents were purchased from Aldrich and used as received without further purification. DMF and other organic solvents were dried and distilled before use. Monomers **1a–1d** were prepared according to the methods reported in the literatures.¹²

Gel permeation chromatography (GPC) was performed in THF at $40\text{ }^\circ\text{C}$ with an elution rate of 1.0 mL min^{-1} on a Waters GPC system equipped with a Waters 486 UV–vis detector, a Waters 515 HPLC pump, a set of Styragel columns (HT3, HT4 and HT6; molecular weight range 10^2 – 10^7), and a column temperature controller. The THF solutions of the polymers (about 2 mg mL^{-1}) were filtered through a $0.45\text{ }\mu\text{m}$ PTFE filter before being injected into the GPC system. IR spectra of the films of the polymers and monomers were recorded on a PerkinElmer 16 PC FTIR spectrophotometer. ^1H and ^{13}C NMR spectra were measured on a Bruker AV 400 spectrometer in deuterated dimethyl sulfoxide, or dichloromethane. Thermogravimetric analysis (TGA) was carried out on a TA TGA Q5000 in nitrogen at a heating rate of $10\text{ }^\circ\text{C/min}$. High-resolution mass spectra (HRMS) were recorded on a GCT premier CAB048 mass spectrometer operated in MALDI-ToF mode. UV spectra were measured on a Milton Ray Spectronic 3000 Array spectrophotometer and photoluminescence (PL) spectra were recorded on a PerkinElmer LS 55 spectrophotometer. Refractive indices (RI) were measured on a J A Woollam Variable Angle Ellipsometry System with a wavelength tunability from 400 to 1000 nm. Photopatterning was conducted in air at room temperature using 365 nm light obtained from a Spectroline

ENF-280C/F UV lamp. Details can be found in our previous publication.¹²

Polymer Synthesis. All the polymerization reactions were performed using the standard Schlenk technique. A typical experimental procedure for the polymerization of **1a**, **2a**, and **3a** is given below as an example. In a 25 mL Schlenk tube equipped with a magnetic stirrer were dissolved **1a** (0.1 mmol), **2a** (0.3 mmol), **3a** (0.6 mmol), PdCl_2 (0.01 mmol), and NaF (0.6 mmol) in distilled DMF (10 mL). The mixture was stirred under nitrogen at $70\text{ }^\circ\text{C}$ for 18 h. Afterward, the polymerization reaction was terminated by pouring the reaction mixture into 150 mL of hexane through a cotton filter to remove insoluble substances, if any formed, and catalyst residues. The precipitates were washed with hexane and dried in vacuum overnight at room temperature until a constant weight was achieved. The polymer was obtained as a yellow powder. Yield: 42.0% (Table S, entry 1). $M_w = 11200$; $M_w/M_n = 3.93$. IR (film), ν (cm^{-1}): 3056 (C=C), 2940 (CH_3), 2866 (CH_2), 1657, 1603, 1510, 1284, 1246, 1175, 1026. ^1H NMR (CD_2Cl_2 , 400 MHz), δ (ppm): 7.50–6.36 (aromatic protons), 3.97–3.87 (OCH_2 protons), 2.30 (CH_3 protons), 1.75 and 1.48 (CH_2 protons). ^{13}C NMR (CD_2Cl_2 , 100 MHz), δ (ppm): 159.80, 133.39, 131.76, 130.98, 130.40, 129.92, 128.39, 115.02, 114.14, 68.19, 29.60, 26.25, 21.31.

P1b/2a/3a. Yellow powder; yield 66.1% (Table S, entry 2). $M_w = 11800$; $M_w/M_n = 2.87$. IR (film), ν (cm^{-1}): 3054 (C=C), 2929 (CH_3), 2857 (CH_2), 1661, 1605, 1509, 1284, 1244, 1175, 1028. ^1H NMR (CD_2Cl_2 , 400 MHz), δ (ppm): 7.51–6.43 (aromatic protons), 3.97–3.76 (OCH_2 protons), 2.45 (CH_3 protons), 2.23, 1.74, and 1.38 (CH_2 protons). ^{13}C NMR (CD_2Cl_2 , 100 MHz), δ (ppm): 159.15, 135.72, 132.99, 131.39, 128.26, 123.59, 114.48, 67.94, 34.19, 30.29, 25.94, 21.86.

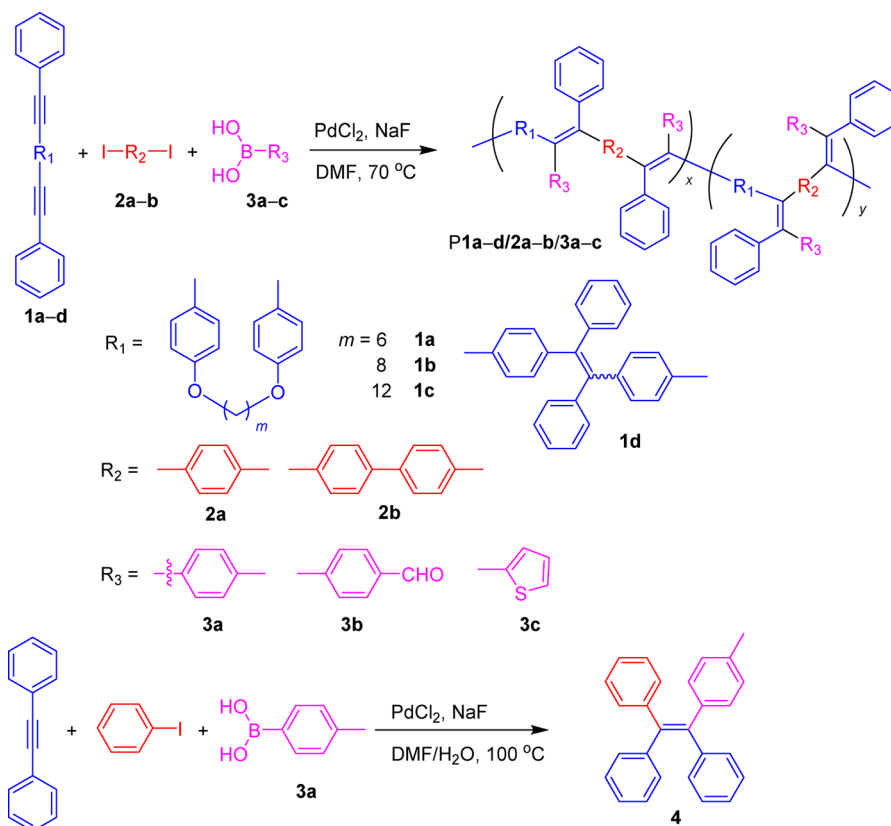
P1c/2a/3a. Yellow powder; yield 43.2% (Table S, entry 3). $M_w = 11100$; $M_w/M_n = 1.72$. IR (film), ν (cm^{-1}): 3054 (C=C), 2927 (CH_3), 2855 (CH_2), 1661, 1603, 1507, 1243, 1175, 1108, 1024. ^1H NMR (CD_2Cl_2 , 400 MHz), δ (ppm): 7.67–6.63 (aromatic protons), 3.97–3.74 (OCH_2 protons), 2.36 (CH_3 protons), 2.29, 1.73, and 1.29 (CH_2 protons). ^{13}C NMR (CD_2Cl_2 , 100 MHz), δ (ppm): 159.17, 135.73, 132.98, 131.39, 128.26, 125.49, 114.48, 67.94, 34.19, 30.29, 29.40, 25.98, 21.16.

P1d/2a/3a. Yellow powder; yield 42.3% (Table S, entry 4). $M_w = 18000$; $M_w/M_n = 2.29$. IR (film), ν (cm^{-1}): 3055 (C=C), 3025 (C=C), 2922 (CH_3), 1663, 1597, 1492, 1442, 1400, 1072, 1023. ^1H NMR (CD_2Cl_2 , 400 MHz), δ (ppm): 7.94–7.11 (aromatic protons), 2.24 (CH_3 protons). ^{13}C NMR (CD_2Cl_2 , 100 MHz), δ (ppm): 143.82, 141.15, 131.66, 128.79, 126.93, 123.60, 121.35, 21.28.

P1a/2a/3b. Yellow powder; yield 62.5% (Table S, entry 5). $M_w = 8900$; $M_w/M_n = 2.19$. IR (film), ν (cm^{-1}): 3055 (C=C), 2937 (CH_3), 2864 (CH_2), 2730 (CHO), 1698 (CHO), 1602, 1508, 1283, 1244, 1014. ^1H NMR (CD_2Cl_2 , 400 MHz), δ (ppm): 10.04 and 9.88 (CHO protons), 8.36–6.39 (aromatic protons), 3.88 (OCH_2 protons), 1.69 and 1.20 (CH_2 protons). ^{13}C NMR (CD_2Cl_2 , 100 MHz), δ (ppm): 162.74, 159.73, 133.34, 131.70, 128.35, 123.96, 115.34, 114.05, 112.91, 68.36, 36.65, 31.47, 29.55, 25.93, 23.95.

P1c/2b/3a. Red solid; yield 72.0% (Table S, entry 6). $M_w = 8000$; $M_w/M_n = 1.70$. IR (film), ν (cm^{-1}): 3055 (C=C), 2924 (CH_3), 2854 (CH_2), 1663, 1609, 1509, 1346, 1247, 1178, 1110, 1022. ^1H NMR (CD_2Cl_2 , 400 MHz), δ (ppm): 7.89–6.61 (aromatic protons), 3.98–3.71 (OCH_2 protons), 2.36 (CH_3 protons), 2.25, 1.84, and 1.29 (CH_2 protons). ^{13}C NMR (CD_2Cl_2 , 100 MHz), δ (ppm): 163.07, 141.42, 138.40, 136.23, 135.19, 134.19, 133.34, 131.70, 128.77, 125.80, 114.94, 68.17, 36.74, 31.52, 30.47, 29.78, 26.34, 25.96, 21.72.

Scheme 3. Palladium-Catalyzed Polycoupling of Internal Diynes, Aryl Diiodides and Aryl Boronic Acids, and Model Reaction

Table 1. Solvent Effect on the Polymerization of 1a, 2a and 3a^a

entry	solvent	temp (°C)	time (h)	yield (%)	M_w	M_w/M_n
1	DMF	70	19	52.7	15100	2.33
2	DMF/H ₂ O ^b	100	48	52.0	12200	2.23
3	THF	100	26	trace		
4	methanol	70	17	trace		
5	toluene	70	17	trace		

^aPolymerization under nitrogen in the presence of 10% of PdCl₂ and 6 equiv of NaF. [1a]:[2a]:[3a] = 1:3:6, [1a] = 0.01 M. ^b4:1 by volume.

P1c/2a/3b. Red solid; yield 40.0% (Table 5, entry 7). $M_w = 4800$; $M_w/M_n = 1.31$. IR (film), ν (cm⁻¹): 3056 (C=C), 2925 (CH₃), 2854 (CH₂), 1601, 1508, 1282, 1174, 1021. ¹H NMR (CD₂Cl₂, 400 MHz), δ (ppm): 10.04 and 9.84 (CHO protons), 7.88–6.40 (aromatic protons), 3.95–3.86 (OCH₂ protons), 1.70–1.28 (CH₂ protons). ¹³C NMR (CD₂Cl₂, 100 MHz), δ (ppm): 133.32, 131.69, 128.58, 114.91, 68.51, 29.75, 26.26.

P1c/2a/3c. Red solid; yield 59.9% (Table 5, entry 8). $M_w = 4700$; $M_w/M_n = 1.21$. IR (film), ν (cm⁻¹): 2954, 2924 (CH₃), 2854 (CH₂), 1604, 1596, 1508, 1458, 1284, 1246, 1173, 1024. ¹H NMR (CD₂Cl₂, 400 MHz), δ (ppm): 7.73–6.60 (aromatic protons), 4.01–3.89 (OCH₂ protons), 1.69, 1.60, 1.42, 1.27, 1.05, and 0.84 (CH₂ protons). ¹³C NMR (CD₂Cl₂, 100 MHz), δ (ppm): 159.84, 133.38, 131.74, 128.79, 124.03, 114.99, 113.94, 111.41, 89.77, 88.25, 68.59, 30.49, 29.70, 27.76, 23.13, 19.93, 14.31.

Model Reaction. Model compound 4 was synthesized by the coupling reaction of diphenylacetylene and 4-methylphenylboronic acid (Scheme 3). The experimental procedure was similar to that for the preparation of P1a/2a/3a except for the fact that DMF/H₂O mixture (4:1 by volume according to the literature⁸) was used as a solvent. Light yellow solid; yield 26% (after purification by silica-gel column chromatography using hexane/ethyl acetate mixture as the eluent). IR (film), ν (cm⁻¹): 3074, 3050, 3020, 1508, 1489, 1442. ¹H NMR (400 MHz, CD₂Cl₂), δ (ppm): 7.09, 7.04, and 6.91 (aromatic protons), 2.26 (s, 3H, CH₃ protons). ¹³C NMR (100 MHz, CD₂Cl₂),

δ (TMS, ppm): 144.00, 140.40, 136.04, 131.28, 128.35, 127.57, 126.26, 21.37. HRMS (MALDI-TOF): m/z 346.1719 (M⁺, calcd 346.4636) (Figure S1 in the Supporting Information).

RESULTS AND DISCUSSION

Polymer Synthesis. To widen the scope of the applicability of polycoupling of internal diyne, aryl diiodide and boronic acid to PTAEs, we optimized the reaction conditions using 1a, 2a, and 3a as model monomers. The effects of different parameters including solvent, temperature, monomer concentration and feeding ratio as well as catalyst loading were examined. The polymerization was first performed in different solvent systems at different temperatures. Since sodium fluoride shows better solubility in water, the model reaction was carried out in a DMF/H₂O mixture as reported (Scheme 3).⁸ However, the polymerization performed in pure DMF gives better results than those in DMF/H₂O mixture (Table 1, entries 1 and 2). The molecular weight of the PTAE produced in pure DMF ($M_w = 15100$) was higher than that ($M_w = 12200$) furnished in a DMF/H₂O mixture. In addition, the use of pure DMF enables the polymerization to perform at a lower temperature and complete in a shorter time, presumably due to the better

solubility of the polymer in this solvent. In contrast, other organic solvents including tetrahydrofuran (THF), methanol and toluene only afford polymers in trace yields (Table 1, entries 3–5). Subsequently, the influence of temperature on the polymerization was investigated. As shown in Table 2,

Table 2. Temperature Effect on the Polymerization of 1a, 2a, and 3a^a

entry	temp (°C)	yield (%)	M_w	M_w/M_n
1	50	48.1	6100	1.56
2 ^b	70	52.7	15100	2.33
3	90	10.4	3400	1.20
4	120	54.6	4800	1.44

^aPolymerization in DMF under nitrogen for 19 h in the presence of 10% equiv of PdCl₂ and 6 equiv of NaF. [1a]:[2a]:[3a] = 1:3:6, [1a] = 0.01 M. ^bData taken from Table 1, entry 1.

increasing the reaction temperature from 70 to 90 °C and then to 120 °C does not improve the yield or the polymerization degree (Table 2, entries 2–4), whereas lowering the temperature to 50 °C decreases the molecular weight of the resulting polymer generated to 6100 (Table 2, entry 1). Such result demonstrates that 70 °C is a suitable temperature for this polymerization.

Traditional polymerization routes involved in preparing PPV require strict stoichiometric control between the two monomer pairs. The reaction developed here, however, is tolerant to stoichiometric imbalance. Theoretically, the molar ratio between 1a, 2a, and 3a was 1:1:2. However, PTAE with the highest molecular weight and yield was obtained at a feed ratio of 1:3:6 (Table 3, entry 1). Thus, an excess amount of

Table 3. Concentration Effect on the Polymerization of 1a, 2a, and 3a^a

entry	[1a]	[2a]	[3a]	yield (%)	M_w ^b	M_w/M_n
1 ^b	0.01	0.03	0.06	52.7	15100	2.33
2	0.01	0.03	0.03	13.2	5500	1.48
3	0.01	0.02	0.06	8.5	5700	1.55
4	0.01	0.02	0.02	11.0	5500	1.40

^aPolymerization at 70 °C in DMF under nitrogen for 19 h in the presence of 10% of PdCl₂. [NaF] = [3a]. ^bData taken from Table 1, entry 1.

aryldiiodide and aryldiboronic acid seems to assist fast and complete consumption of the diyne monomer. It is worthy to note that even when a low monomer concentration 0.01 M was used, the polymerization also proceeds well.

Palladium complexes are found to be efficient for catalyzing the coupling reactions of alkyne, aryl iodides and arylboronic acids.¹³ We examined the efficiency of several commonly used palladium complexes in order to select the most suitable one for our system. Regarding the molecular weights of the polymers generated, we found that PdCl₂ at a loading of 10% outperformed its cousins (Table 4, entry 1). Reducing the loading from 10% to 5% generates a polymer in a higher yield (59.3%), but with a poorer solubility, probably due to the formation of high molecular weight species. On the other hand, raising the catalyst loading leads to a poorer result in terms of lower yield and molecular weight (Table 4, entry 3). Thus, 10% PdCl₂ was chosen for catalyzing the polymerization in the subsequent research.

Table 4. Effects of Different Catalysts and Loading on the Polymerization of 1a, 2a and 3a^a

entry	catalyst	loading (%)	yield (%)	M_w	M_w/M_n	S^b
1	PdCl ₂	10	42.0	10000	1.90	√
2	PdCl ₂	5	59.3	7300	1.75	Δ
3	PdCl ₂	20	25.3	6600	1.61	√
4	Pd(OAc) ₂	10	~100	3400	1.16	√
5	[Pd(PPh ₃) ₂ Cl ₂]	10	16.8	3600	1.19	√

^aPolymerization at 70 °C in DMF under nitrogen for 18 h (entries 1–3) and 19 h (entries 4 and 5) in the presence of 10% of catalyst and 6 equiv of NaF. [1a]:[2a]:[3a] = 1:3:6, [1a] = 0.01 M. ^bSolubility (S) tested in common organic solvents, such as dichloromethane, chloroform, and tetrahydrofuran: √ = completely soluble, Δ = partially soluble.

On the basis of the investigation above, we explored the monomer scope in order to enrich the molecular structures and introduce functionality to the polymers. We performed polymerizations using aromatic internal diynes 1a–1d with different alkyl chain lengths or TPE luminogenic unit, aryl diiodides 2a–2b and arylboronic acids 3a–3c carrying different aryl rings. All the reactions proceed smoothly, generating polymers with moderate to high molecular weights (M_w = 4700–18000) in moderate yields (40.0–72.0%) (Table 5).

Table 5. Polymerization of Different Monomers^a

entry	monomer	[1] (M)	yield (%)	M_w	M_w/M_n	S^b
1	1a/2a/3a	0.01	42.0	11200	3.93	√
2	1b/2a/3a	0.02	66.1	11800	2.87	√
3	1c/2a/3a	0.02	43.2	11100	1.72	√
4	1d/2a/3a	0.01	42.3	18000	2.29	√
5	1a/2a/3b	0.01	62.5	8900	2.19	√
6	1c/2b/3a	0.02	72.0	8000	1.70	Δ
7	1c/2a/3b	0.02	40.0	4800	1.31	Δ
8	1c/2a/3c	0.02	59.9	4700	1.21	Δ

^aPolymerization at 70 °C in DMF under nitrogen for 18 h in the presence of 10% equiv of catalyst and 6 equiv of NaF. [1]:[2]:[3] = 1:3:6. ^bSolubility (S) tested in common organic solvents, such as dichloromethane, chloroform, and tetrahydrofuran: √ = completely soluble, Δ = partially soluble.

Most of the polymers are soluble in common organic solvents, except those synthesized from 1c, which may possess a high molecular weight and hence a low solubility (Table 5, entries 6–8). The moderate yields may be attributed to the production of terphenyl derivatives as byproducts from the Suzuki coupling of aryl diiodides and arylboronic acids.

Structural Characterization. We utilized IR and NMR techniques to characterize the polymers obtained and model compound. The IR spectra of polymer P1a/2a/3a and its monomers 1a, 2a, and 3a as well as the model compound 4 are given in Figure 1. The CH₂ and C–O–C stretching vibrations of 1a are observed at 2941 and 1246 cm⁻¹, which are also found in the spectrum of P1a/2a/3a. On the other hand, the spectra of 4 and P1a/2a/3a show no absorption band at 1346 cm⁻¹ related to the B–O stretching vibration of 3a. They both exhibit C=C stretching absorption bands at around 3050 cm⁻¹ originated from the transformation of the C≡C triple bonds of 1a by the polymerization reaction.

Analysis by ¹H NMR spectroscopy gives more detailed structural information. Figure 2 depicts the ¹H NMR spectra of

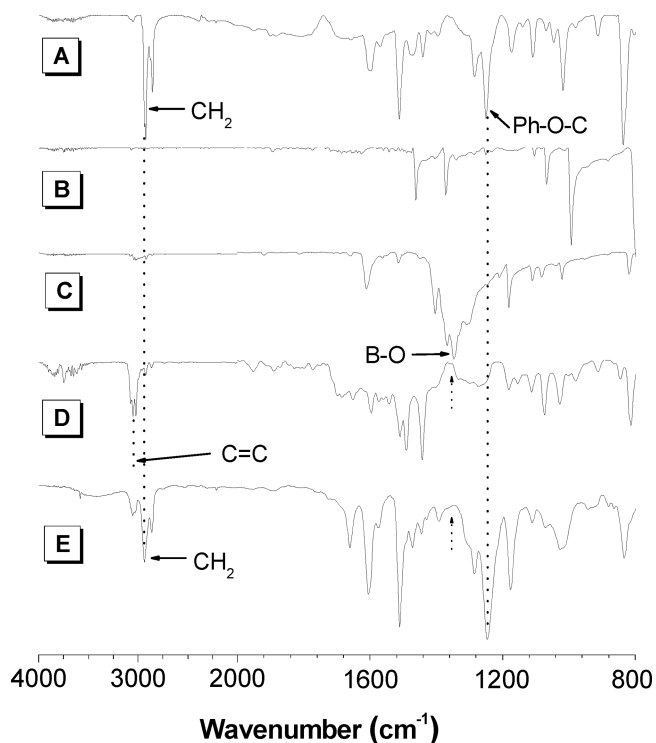


Figure 1. IR spectra of (A) **1a**, (B) **2a**, (C) **3a**, (D) **4**, and (E) **P1a/2a/3a**.

monomers **1a**, **2a**, and **3a**, model compound **4**, and polymer **P1a/2a/3a**. The methylene protons of **1a** resonate at δ 3.99, 1.84 and 1.55, which are also found at the same positions in the spectrum of **P1a/2a/3a** (Figure 2, parts A and E). The absorption of the methyl group of **3a**, on the other hand, upfield-shifts from δ 2.44 to 2.25 after the model reaction and polymerization (Figure 2, parts C–E). Meanwhile, the spectra of **4** and **P1a/2a/3a** exhibit no resonance of the boronic acid protons of **3a** at δ 8.14. This suggests the complete consumption of the boronic acid group by the polymerization. The ^{13}C NMR spectrum of **P1a/2a/3a** is given in Figure S2. The spectrum of the polymer shows no triple bond resonances of **1a** at δ 89.82 and 88.18. Instead, it exhibits a peak related to the methyl carbon absorption of **3a** at δ 21.52. No unexpected signals are detected and all the peaks can be readily assigned by comparing the spectrum with those of its monomers and model compound. Thus, all the ^1H NMR and ^{13}C NMR data prove that the polymeric product is indeed **P1a/2a/3a**, with a molecular structure as shown in Scheme 3. The IR and NMR data of other polymers are summarized in the Experimental Section and all confirm their expected molecular structures.

Thermal Stability. High thermal stability is usually a prerequisite for polymers to be served as functional materials. Figure 3 shows the thermal stability of the PTAEs evaluated by TGA analysis. Most of the polymers retain 30–75% of their weights after being heated to 800 °C under nitrogen and show merely 5% weight loss at temperatures between 212–67 °C (T_d). These render them as potential candidates for heat-resistant materials.

Optical Properties. Because of their diverse structures, polymers **P1/2/3** exhibit different optical properties. Figure 4A shows the absorption spectra of the polymers in THF solutions. Among the polymers, **P1a/2a/3b** shows the longest absorption maximum wavelength at 370 nm, probably due to the

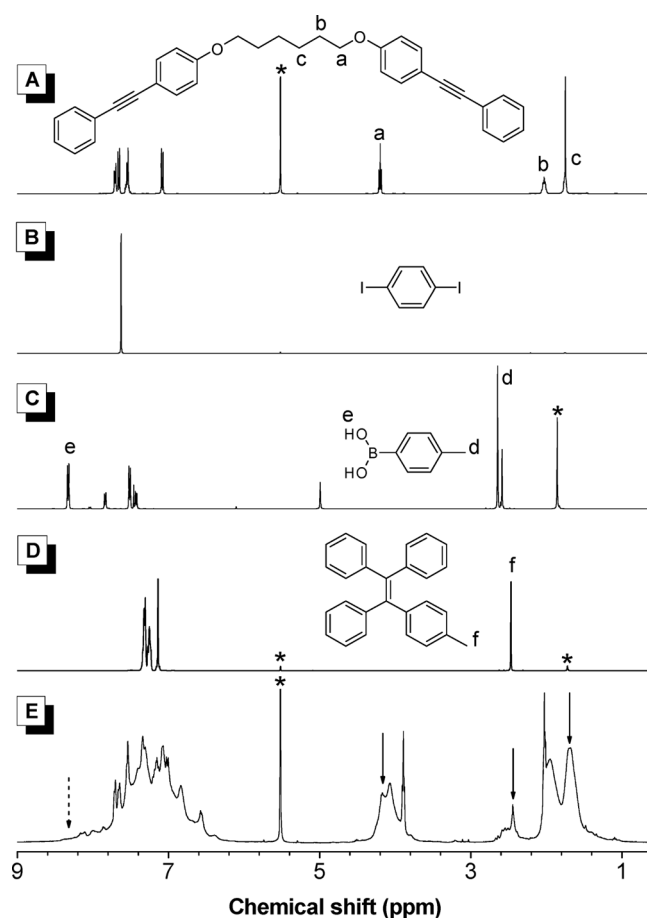


Figure 2. ^1H NMR spectra of (A) **1a**, (B) **2a**, (C) **3a**, (D) **4**, and (E) **P1a/2a/3a** in (A, B, D and E) CD_2Cl_2 and (C) $(\text{CD}_3)_2\text{SO}$. The solvent peaks are marked with asterisks.

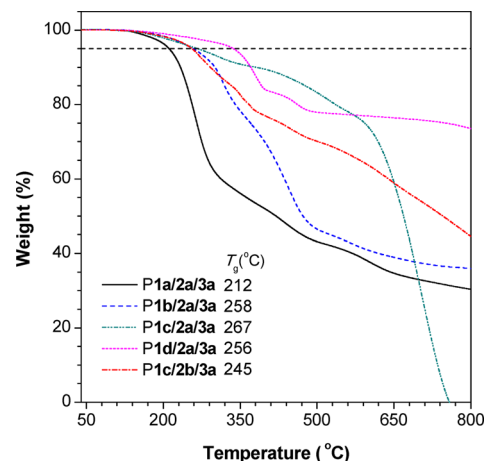


Figure 3. TGA thermograms of **P1a–1d/2a–2b/3a** recorded under nitrogen at a heating rate of 10 °C/min.

intramolecular charge transfer (ICT) from the electron-rich tetraarylethene unit to the electron-withdrawing aldehyde group. The absorption maximum of other polymers locate within a wavelength range of 325–358 nm (Table 6). **P1a/2a/3a** shows a bluer absorption than **P1d/2a/3a** because of its nonfully conjugated structure but absorbs at longer wavelength than **P1c/2b/3a** because its tetraarylethene moiety may take a more planar conformation due to the lesser steric hindrance

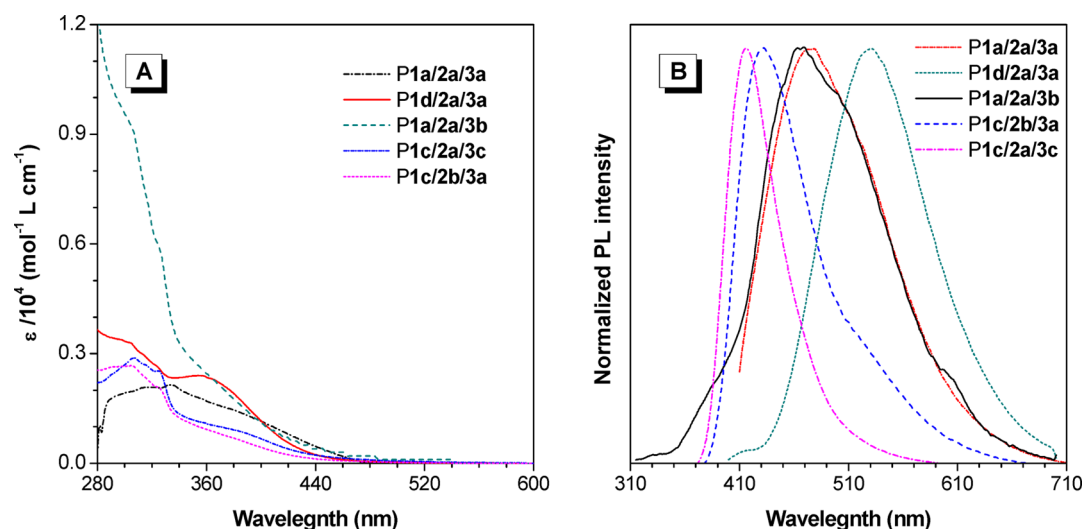


Figure 4. (A) Absorption spectra and (B) normalized PL spectra of P1/2/3 in THF solutions. Excitation wavelength (nm): 340 (P1a/2a/3a), 358 (P1d/2a/3a), 370 (P1a/2a/3b), 325 (P1c/2a/3c), and 326 (P1c/2b/3a).

Table 6. Optical Properties of P1/2/3^a

polymer	λ_{abs} (nm)	λ_{em} (nm)
P1d/2a/3a	358	531
P1a/2a/3a	340	478
P1a/2a/3b	370	469
P1c/2a/3c	325	416
P1c/2b/3a	326	433

^aIn dilute THF solution. Abbreviation: λ_{abs} = absorption maximum; λ_{em} = emission maximum.

between the aryl rings. The corresponding PL spectra are shown in Figure 4B. Instead of P1a/2a/3b, whose PL is sensitive to the solvent polarity, the emission maximum of other polymers seems to be correlated with their conjugation, with 1d/2a/3a being the reddest emitter.

Tetraphenylethene (TPE) is a luminogen with AIE characteristic. Being a TPE derivative, model compound 4 is anticipated to be also AIE-active.¹⁴ It is really the case. As

shown in Figure 5, the THF solution of 4 was barely emissive under photoexcitation at 312 nm. Addition of a large amount of water, a poor solvent for 4, into its THF solution aggregate its molecules and induces it to emit intensity. Clearly, 4 exhibits the AIE phenomenon.

The luminogenic units of polymers P1a/2a/3a and P1d/2a/3a are similar to 1,4-bis(1,2,2-triphenylvinyl)benzene, an AIE luminogen.¹⁶ Thus, both polymers are anticipated to show strong emission in the aggregated state. Unlike 4, both P1a/2a/3a and P1d/2a/3a are somewhat emissive in their THF solutions albeit with a weak intensity. We have proposed that the restriction of intramolecular motion (RIM)¹⁵ is the main cause for the AIE effect. The AIE units in the polymers are linked by covalent bonds and suffer certain steric effect from its neighbors. These activate their RIM process and thus enable the polymers to show somewhat light emission in the solution state (Figure 6). The formation of nanoaggregates upon water addition into the polymer solutions has further enhanced the emission intensity. Interestingly, at water content exceeded 80

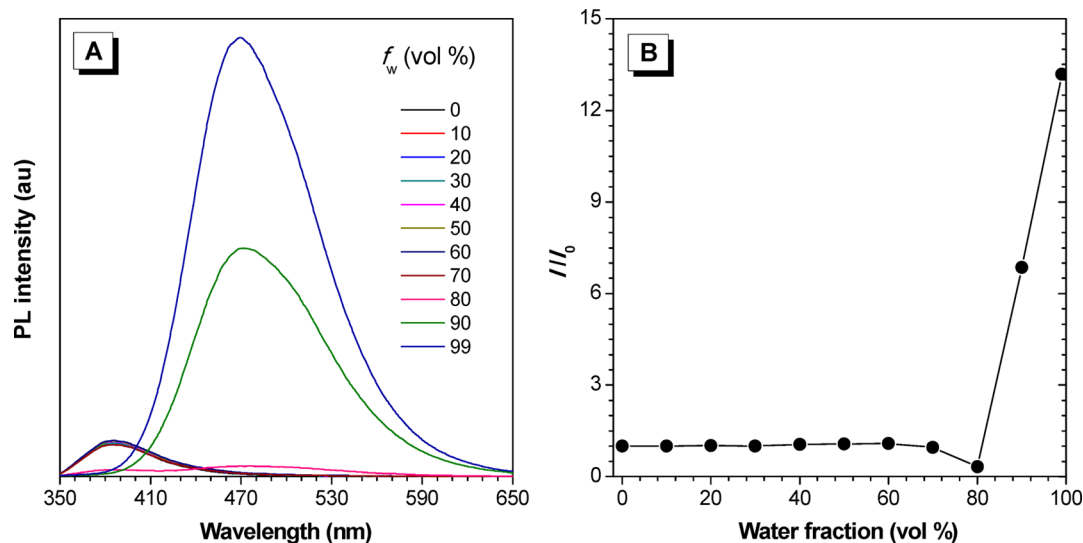


Figure 5. (A) PL spectra of 4 in THF and THF/H₂O mixtures with different water fractions (f_w). Concentration: 10 μM . Excitation wavelength: 312 nm. (B) Plot of relative PL intensity (I/I_0) versus the composition of the THF/H₂O mixture of 4.

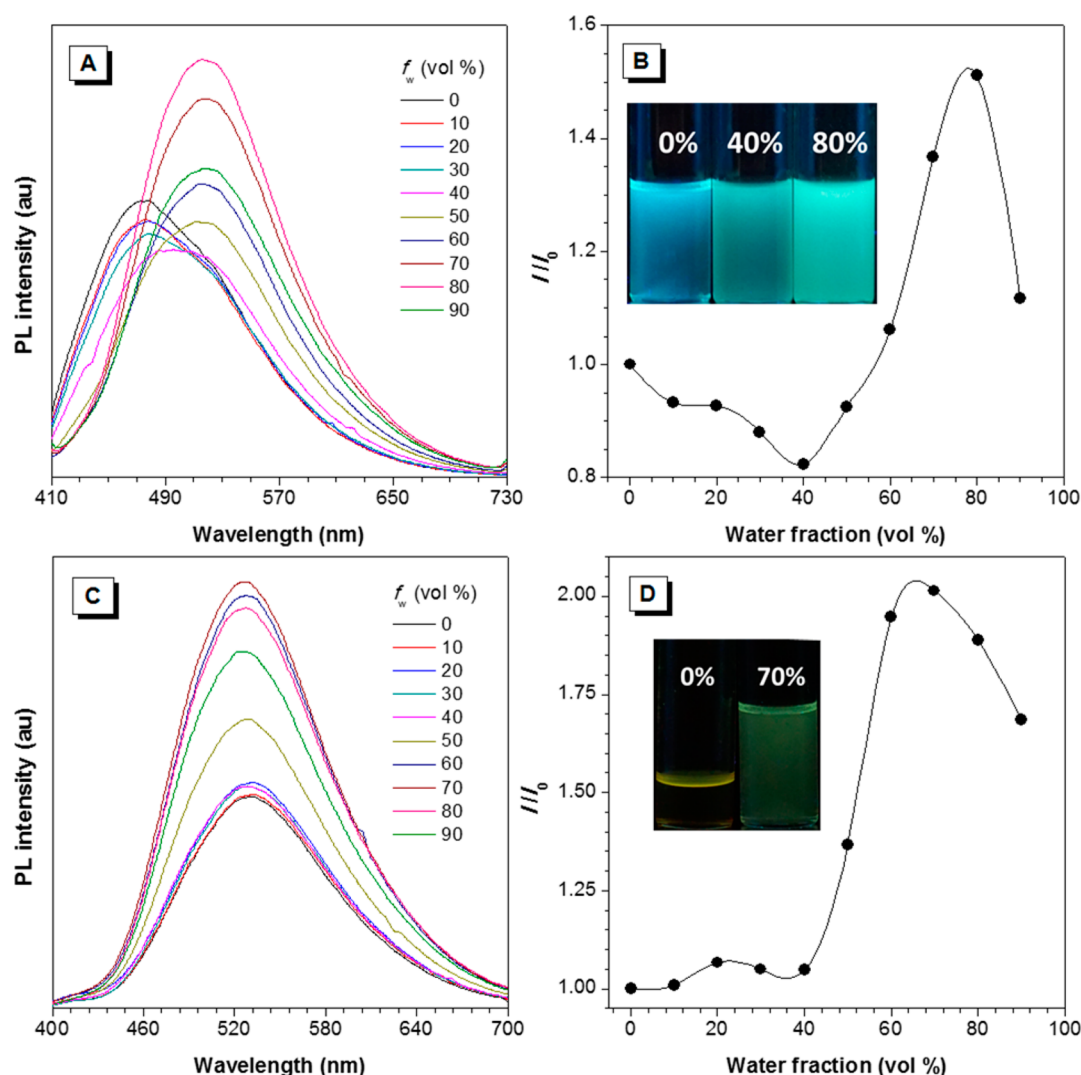


Figure 6. PL spectra of (A) P1a/2a/3a and (C) P1d/2a/3a in THF and THF/H₂O mixtures with different water fractions (f_w). Concentration (μM): 20 (P1a/2a/3a) and 10 (P1d/2a/3a); excitation wavelength (nm): 340 (P1a/2a/3a) and 358 (P1d/2a/3a). (B and D) Plot of the relative PL intensity (I/I_0) as a function of the water fraction in the THF/H₂O mixture of (B) P1a/2a/3a and (D) P1d/2a/3a. Insets in parts B and D: fluorescent photos of P1a/2a/3a and P1d/2a/3a in THF/H₂O mixtures with different f_w .

vol % for P1a/2a/3a and above 70 vol % for P1d/2a/3a, their emission becomes weaker. Such a phenomenon may result from the formation of large aggregates in the presence of water, which reduces the effective solute concentration. P1d/2a/3a emits at a longer wavelength (529 nm) than P1a/2a/3a (478 nm), probably due to its higher conjugation.

We also investigated the optical properties of P1a/2a/3b, P1c/2a/3c, and P1c/2b/3a in THF/water mixture. Unlike P1a/2a/3a and P1d/2a/3a, the strong emission of these polymers in THF is quenched upon aggregate formation in the presence of water (Figures S3–S5). The higher the water content in the THF/water mixture, the weaker is the light emission. The enhancement of the ICT effect by increasing the solvent polarity upon water addition in P1a/2a/3b may be responsible for the emission quenching. The thiophene ring and triphenylethene unit in P1c/2a/3c may serve as energy acceptor and donor, respectively.¹⁷ When they are in close proximity in the aggregates, it may lead to emission quenching via the Förster resonance energy transfer mechanism. The volume shrinkage of the polymer chain of P1c/2b/3a in the presence of poor solvent may push the phenyl rings in close

vicinity. This enhances their π – π stacking interactions and results in PL annihilation. On the other hand, the RIM process is activated upon aggregate formation, which results in emission enhancement. The first factor seems to be predominant in P1c/2b/3a in the aggregated state and thus the observation of PL drop upon gradual addition of water.

Metal Ion Detection. Ruthenium(III) complexes are commonly used catalysts for many oxidation,¹⁸ metathesis,¹⁹ and reduction²⁰ reactions, but they can potentially cause corrosion and are irritating to skin, the eyes, and the respiratory and digestive systems. Therefore, detection and monitoring of ruthenium(III) ions has become an important safety issue. However, few papers are available in the literature dealing with the quantitative fluorescence detection for Ru³⁺.^{16,21,22} Taking advantages of the high sensitivity, reliability, and selectivity of fluorescent sensors and the AIE property of polymer P1d/2a/3a, we investigated its potential as a fluorescent chemosensor for Ru³⁺ ion.

The emission spectra of P1d/2a/3a in THF/H₂O mixtures (3:7 v/v) containing different amounts of RuCl₃ are given in Figure 7A. With an increase in the concentration of Ru³⁺ from

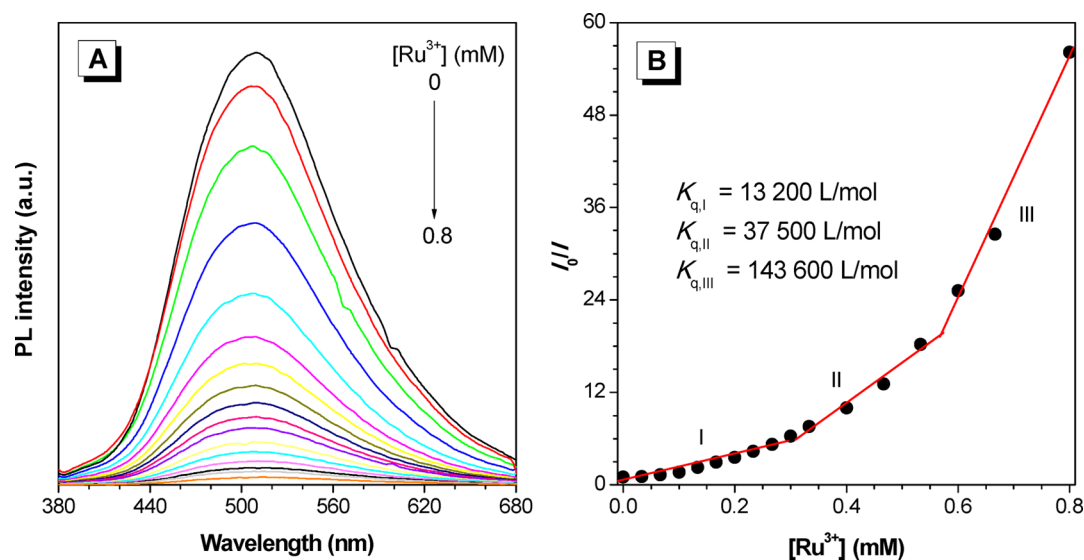


Figure 7. (A) PL spectra of **P1d/2a/3a** in THF/H₂O mixtures (3:7 v/v, 10 μM) containing different amounts of Ru³⁺. (B) Stern–Volmer plots of relative intensity (I_0/I) versus the Ru³⁺ concentration. I_0 = PL intensity in the absence of Ru³⁺.

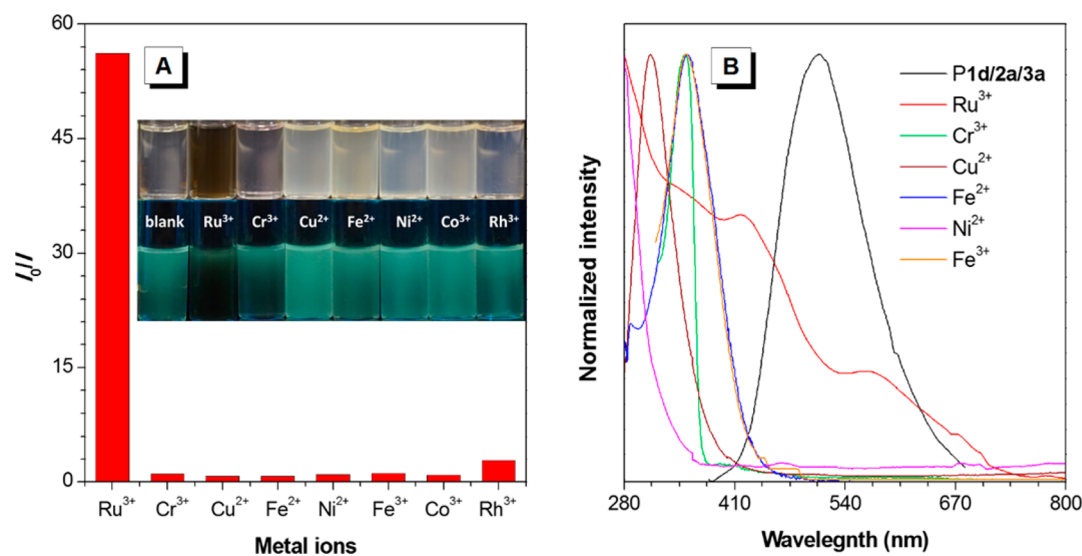


Figure 8. (A) Selectivity of **P1d/2a/3a** to different metal ions (0.8 mM in THF) in THF/H₂O mixture (3:7 by volume, 10 μM). I_0 = intensity in the absence of metal ions. Inset: Photographs of **P1d/2a/3a** in THF/H₂O mixtures (3:7 by volume) containing different metal ions taken under (upper) daylight and (lower) UV illumination. (B) Normalized emission spectrum of **P1d/2a/3a** in THF/H₂O mixture (3:7 by volume) and absorption spectra of metal ions. Concentration: 10 μM (**P1d/2a/3a**) and 1 mM (metal ions).

0 to 0.8 mM, the emission of the polymer aggregates was gradually quenched while the spectral profile remained unchanged. The Stern–Volmer plots of relative PL intensity (I_0/I) versus the Ru³⁺ concentration provides a more detailed picture of the quenching process (Figure 7B). At different metal ion concentrations, the quenching constants deduced from the linear region of the plot varies from 13200 M⁻¹ (0–0.3 mM), to 37500 M⁻¹ (0.3–0.6 mM) and then 143600 M⁻¹ (0.6–0.8 mM). This trend shows that at high Ru³⁺ concentration, the sensing performance of the polymer becomes higher. Such amplification is attributed to an increase in the number of binding cavity due to the conformational change caused by Ru³⁺ ions already bound to the polymer.

In order to investigate the selectivity of the metal ion sensor, we tested the emission response of the polymer to several other ions, including Cr³⁺, Cu²⁺, Fe³⁺, Fe²⁺, Ni²⁺, Co³⁺, Rh³⁺, Ag⁺, Hg²⁺, and Zn²⁺. Figure 8A illustrates the relative intensity (I_0/I)

of **P1d/2a/3a** in THF/H₂O mixtures (3:7 by volume) with 0.8 mM of some of these cations. Results show that the emission of **P1d/2a/3a** is only sensitive to the presence of Ru³⁺ ion, which is demonstrative of the high specificity of the fluorescent chemosensor. Different mechanisms have been proposed for such selectivity, such as high reduction potential of Ru³⁺ ion,^{16a,17,22} heteroatom-involved energy transfer²¹ and formation of metal complex or coordination effect.²³ In this case, the dark color of the aqueous solution of RuCl₃ gives us a hint that its absorption may be responsible for the emission annihilation. Thus, we studied the electronic transitions of RuCl₃ and other metal ions for comparison. As shown in Figure 8B, the absorption spectrum of Ru³⁺ overlaps with the emission spectrum of **P1d/2a/3a** at the wavelength range of 400–670 nm. This will lead to the energy transfer from the excited state of the polymer to the ground state of Ru³⁺ and hence quench its emission. In contrast, the onset wavelength of the absorption

spectra of other metal ions is all shorter than 410 nm. Thus, efficient energy transfer between them and the polymer aggregates is less likely to occur.

Light Refraction. Polymers with high refractive indices (RI) are promising candidates for a variety of photonic applications, such as organic light-emitting diodes, waveguides, lenses and image sensors.²⁴ Theoretically, polymers with heteroatoms, polarized aromatic rings and large conjugation are likely to exhibit high RI values. Our polymers can be fabricated into uniform films on silica wafers by drop-casting or spin-coating with thicknesses of 100–300 nm. Their films exhibit RI of 1.6382–1.7751 at 632.8 nm, whose values are higher than those of commercial polymers such as polycarbonate ($n = 1.593$ – 1.576) and polystyrene ($n = 1.602$ – 1.589) (Figure 9).²⁵ In particular, polymer **P1d/2a/3a** exhibits the

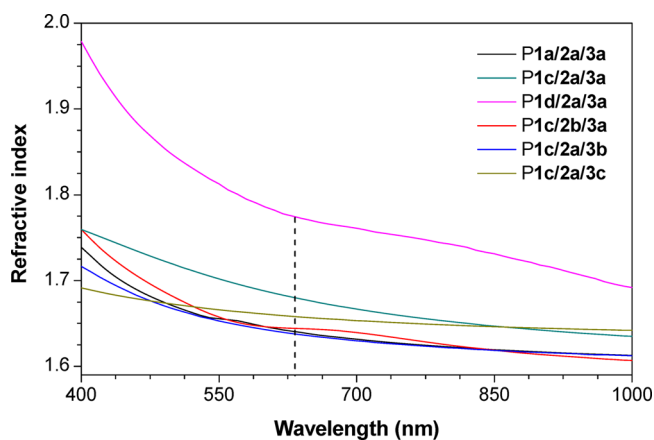


Figure 9. Wavelength-dependent refractive indices of thin films of **P1a-d/2a-b/3a-c**.

highest RI values of 1.9788–1.6917 in the range of 400–1000 nm, thanks to its fully conjugated backbone. The high RI values of **P1/2/3** enable them to be used in a variety of above-mentioned applications.

Chromatic Dispersion. Chromatic dispersion (D) of a particular material is related to its wavelength-dependent refractive index. The Abbé number (ν_D) describes the variation of RI as a function of the wavelength. Those with high D values are not favorable in fabricating optical devices since they will lead to chromic aberration.²⁶ As shown in Table 7, the ν_D and the corresponding D values of the polymers fall in the range of 7.4574–36.7667 and 0.0272–0.1341, respectively. Obviously, the high RI values and low dispersion of the polymers endow

Table 7. Refractive Indices and Chromatic Dispersions of **P1/2/3**^a

polymer	$n_{632.8}$	ν_D	D
P1a/2a/3a	1.6409	16.9034	0.0592
P1c/2a/3a	1.6806	12.2429	0.0817
P1d/2a/3a	1.7751	7.4575	0.1341
P1c/2b/3a	1.6445	14.7808	0.0677
P1c/2a/3b	1.6382	17.7115	0.0565
P1c/2a/3c	1.6583	36.7667	0.0272

^aAbbreviation: n = refractive index, ν_D = Abbé number = $(n_D - 1)/(n_F - n_C)$, where n_D , n_F , and n_C are the RI values at wavelengths of Fraunhofer D, F, and C spectral lines of 589.2, 486.1, and 656.3 nm, respectively; $D = 1/\nu_D$.

them with many advanced applications such as high-performance complementary metal-oxide-semiconductor image sensors.²⁴

Photopatterning. **P1d/2a/3a** possesses a good film-forming capacity and exhibits strong emission in the solid state. These properties make it promising for the facile fabrication of nanoscale luminescent patterns. The spin-coated film of **P1d/2a/3a** on a silicon wafer was illuminated through a copper mask by UV light for 10 min. As depicted in Figure 10,

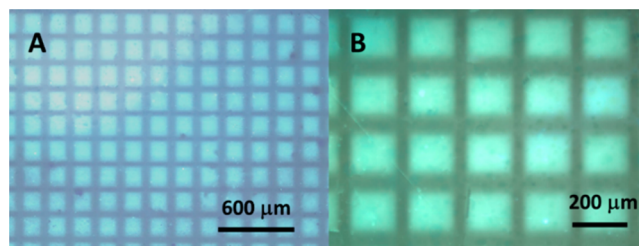


Figure 10. Photopatterns generated by photolithography of a film of **P1d/2a/3a** through a copper mask taken under (A) normal light illumination and (B) UV irradiation. Excitation wavelength: 330–385 nm.

the exposed parts (lines) of the films are photobleached and thus appear dark upon UV irradiation, while the unexposed squares still emit brightly.^{10a} High resolution patterns are thus discernible under normal light illumination and UV irradiation. Therefore, this technique proves to be highly efficient and facile for the construction of photonic and electronic devices as well as biological sensing and probing systems.²⁷

CONCLUSIONS

We have successfully developed a highly efficient approach to prepare poly(tetraarylethene)s by a one-pot one-step palladium-catalyzed three-component polycondensation of internal diynes, aryl diiodides, and arylboronic acids. This polymerization enjoys the advantages of mild reaction condition, less costly catalyst,²⁸ and a high tolerance to different functional groups. The obtained polymers possess distinguished properties such as good film-forming capability, high refractive indices and good thermal stability. The strong aggregate/solid state-emission characteristic of TPE-containing PTAE enables it to be a promising material for fabricating high-resolution photopatterns and serve as a highly sensitive and selective fluorescent chemosensor for Ru^{3+} ion. Therefore, this paper demonstrates a successful strategy for manipulating the properties and functionalities of polymers via proper structural design. Further research will be directed to explore monomers with other functional groups, such as pyrrole and fluorophenyl rings and potential applications of the resulting polymers as electrofluorescent materials for PLED.

ASSOCIATED CONTENT

Supporting Information

The Supporting Information is available free of charge on the ACS Publications Web site. The Supporting Information is available free of charge on the ACS Publications website at DOI: 10.1021/acs.macromol.5b01946.

HRMS spectrum of **4**, ¹³C NMR spectra of **1a**, **2a**, **3a**, **4** and **P1a/2a/3a**, and PL spectra of **P1a/2a/3b**, **P1c/2a/3c**, and **P1c/2b/3a** (PDF)

■ AUTHOR INFORMATION

Corresponding Author

*(B.Z.T.) E-mail: tangbenz@ust.hk. Telephone: +852-2358-7375. Fax: +852-2358-1594.

Notes

The authors declare no competing financial interest.

■ ACKNOWLEDGMENTS

This work was partially supported by the National Basic Research Program of China (973 Program; 2013CB834701), the National Science Foundation of China (21490570 and 21490574), the University Grants Committee of Hong Kong (AoE/P-03/08), the Research Grants Council of Hong Kong (16305014, 16303815 and 604913), and the Nissan Chemical Industries, Ltd. B.Z.T. expresses thanks for the support of the Guangdong Innovative Research Team Program (201101C0105067115).

■ REFERENCES

- (1) (a) Wu, W.; Tang, R.; Li, Q.; Li, Z. *Chem. Soc. Rev.* **2015**, *44*, 3997–4022. (b) Heeger, A. J. *Rev. Mod. Phys.* **2001**, *73*, 681–700. (c) Feast, W. J.; Tsibouklis, J.; Pouwer, K. L.; Groenendaal, L.; Meijer, E. W. *Polymer* **1996**, *37*, 5017–5047.
- (2) Burroughes, J.; Bradley, D.; Brown, A.; Marks, R.; Mackay, K.; Friend, R.; Burns, P.; Holmes, A. *Nature* **1990**, *347*, 539–541.
- (3) Gustafsson, G.; Cao, Y.; Treacy, G.; Klavetter, F.; Colaneri, N.; Heeger, A. *Nature* **1992**, *357*, 477–479.
- (4) Wang, L.; Li, H.; Cao, D. *Curr. Org. Chem.* **2012**, *16*, 1468–1484.
- (5) Huang, M. H.; Tian, Z. F.; Huang, H. *Adv. Mater. Res.* **2013**, *643*, 13–16.
- (6) (a) Yang, S. H.; Hsu, C. S. *J. Polym. Sci., Part A: Polym. Chem.* **2009**, *47*, 2713–2733. (b) Chen, S.-A.; Chang, E.-C. *Macromolecules* **1998**, *31*, 4899–4907.
- (7) Díaz, C.; Alzate, D.; Rodríguez, R.; Ochoa, C.; Sierra, C. A. *Synth. Met.* **2013**, *172*, 32–36.
- (8) (a) Zhou, C.; Larock, R. C. *J. Org. Chem.* **2005**, *70*, 3765–3777. (b) Zhou, C.; Emrich, D. E.; Larock, R. C. *Org. Lett.* **2003**, *5*, 1579–1582.
- (9) Nakagawa, K.; Tomita, I. *Chem. Lett.* **2007**, *36*, 638–639.
- (10) (a) Liu, Y.; Zhao, Z.; Lam, J. W. Y.; Zhao, Y.; Chen, Y.; Liu, Y.; Tang, B. Z. *Macromolecules* **2015**, *48*, 4241–4249. (b) Gao, M.; Lam, J. W. Y.; Li, J.; Chan, C. Y. K.; Chen, Y.; Zhao, N.; Han, T.; Tang, B. Z. *Polym. Chem.* **2013**, *4*, 1372–1380. (c) Gao, M.; Lam, J. W. Y.; Liu, Y.; Li, J.; Tang, B. Z. *Polym. Chem.* **2013**, *4*, 2841–2849.
- (11) (a) Mei, J.; Hong, Y.; Lam, J. W. Y.; Qin, A.; Tang, Y.; Tang, B. Z. *Adv. Mater.* **2014**, *26*, 5429–5479. (b) Hong, Y.; Lam, J. W. Y.; Tang, B. Z. *Chem. Soc. Rev.* **2011**, *40*, 5361–5388.
- (12) Liu, Y.; Gao, M.; Lam, J. W. Y.; Hu, R.; Tang, B. Z. *Macromolecules* **2014**, *47*, 4908–4919.
- (13) Flynn, A. B.; Ogilvie, W. W. *Chem. Rev.* **2007**, *107*, 4698–4745.
- (14) (a) Hong, Y.; Lam, J. W. Y.; Tang, B. Z. *Chem. Commun.* **2009**, *29*, 4332–4353. (b) Luo, J. D.; Xie, Z. L.; Lam, J. W. Y.; Cheng, L.; Chen, H. Y.; Qiu, C. F.; Kwok, H. S.; Zhan, X. W.; Liu, Y. Q.; Zhu, D. B.; Tang, B. Z. *Chem. Commun.* **2001**, 1740–1741.
- (15) Mei, J.; Hong, Y.; Lam, J. W. Y.; Qin, A.; Tang, Y.; Tang, B. Z. *Adv. Mater.* **2014**, *26*, 5429–5479.
- (16) (a) Chan, C. Y. K.; Zhao, Z.; Lam, J. W. Y.; Liu, J.; Chen, S.; Lu, P.; Mahtab, F.; Chen, X.; Sung, H. H. Y.; Kwok, H. S.; Ma, Y.; Williams, I. D.; Wong, K. S.; Tang, B. Z. *Adv. Funct. Mater.* **2012**, *22*, 378–389. (b) Wang, W.; Lin, T.; Wang, M.; Liu, T.-X.; Ren, L.; Chen, D.; Huang, S. J. *Phys. Chem. B* **2010**, *114*, 5983–5988.
- (17) Finazzi Agrò, A.; Federici, G.; Giovagnoli, C.; Cannella, C.; Cavallini, D. *Eur. J. Biochem.* **1972**, *28*, 89–93.
- (18) (a) Murahashi, S.-I.; Komiyama, N. *Ruthenium-Catalyzed Oxidation for Organic Synthesis. In Modern Oxidation Methods*; Wiley-VCH Verlag GmbH & Co. KGaA: Weinheim, Germany, 2010; 241–275.
- (b) Sharpless, K. B.; Akashi, K.; Oshima, K. *Tetrahedron Lett.* **1976**, *17*, 2503–2506.
- (19) (a) Nelson, D. J.; Manzini, S.; Urbina-Blanco, C. A.; Nolan, S. P. *Chem. Commun.* **2014**, *50*, 10355–10375. (b) Fürstner, A. *Ruthenium-Catalyzed Metathesis Reactions in Organic Synthesis. In Alkene Metathesis in Organic Synthesis*, Fürstner, A., Ed. Springer: Berlin and Heidelberg, Germany, 1998; *1*, 37–72.
- (20) (a) Bontemps, S.; Vendier, L.; Sabo-Etienne, S. *J. Am. Chem. Soc.* **2014**, *136*, 4419–4425. (b) Gutsulyak, D. V.; Nikonov, G. I. *Adv. Synth. Catal.* **2012**, *354*, 607–611. (c) Fukuzawa, H.; Ura, Y.; Kataoka, Y. *J. Organomet. Chem.* **2011**, *696*, 3643–3648.
- (21) Deng, H.; Hu, R.; Zhao, E.; Chan, C. Y. K.; Lam, J. W. Y.; Tang, B. Z. *Macromolecules* **2014**, *47*, 4920–4929.
- (22) Chan, C. Y. K.; Lam, J. W. Y.; Jim, C. K. W.; Sung, H. H. Y.; Williams, I. D.; Tang, B. Z. *Macromolecules* **2013**, *46*, 9494–9506.
- (23) Kangwanwong, T.; Pluempanupat, W.; Parasuk, W.; E. Keenan, H.; Songsasen, A. *ScienceAsia* **2012**, *38*, 278–282.
- (24) Liu, J.; Ueda, M. *J. Mater. Chem.* **2009**, *19*, 8907–8919 and references therein.
- (25) (a) Mills, N. J. *Concise Encyclopedia of Polymer Science & Engineering*; Kroschwitz, J. I., Ed.; Wiley: New York, 1990; pp 683–687. (b) Seferis, J. C. *Polymer Handbook*, 3rd ed.; Brandrup, J., Immergut, E. H., Eds.; Wiley: New York, 1989; pp VI/451–VI/461.
- (26) Hecht, E. *Optics*, 4th ed.; Addison Wesley: San Francisco, CA, 2002.
- (27) (a) Kim, J. M. *Macromol. Rapid Commun.* **2007**, *28*, 1191–1212. (b) Campbell, M.; Sharp, D. N.; Harrison, M. T.; Denning, R. G.; Turberfield, A. J. *Nature* **2000**, *404*, 53–56.
- (28) Prices offered by Sigma-Aldrich online supplier: www.sigmaaldrich.com.